nature genetics

LETTERS

https://doi.org/10.1038/s41588-018-0287-5

Acquired HER2 mutations in ER+ metastatic breast cancer confer resistance to estrogen receptor–directed therapies

Utthara Nayar[1,2,3,4,9], Ofir Cohen[1,2,3,4,9], Christian Kapstad[1,2,4], Michael S. Cuoco[5], Adrienne G. Waks[1,2,3,4,6], Seth A. Wander[1,2,3,4,6], Corrie Painter[4], Samuel Freeman[2,3,4], Nicole S. Persky[4], Lori Marini[1,2], Karla Helvie[1,2], Nelly Oliver[1,2], Orit Rozenblatt-Rosen[5], Cynthia X. Ma[7], Aviv Regev[5,8], Eric P. Winer[2,3,6], Nancy U. Lin[2,3,6] and Nikhil Wagle[1,2,3,4,6*]

Seventy percent of breast cancers express the estrogen receptor (ER), and agents that target the ER are the mainstay of treatment. However, virtually all people with ER+ breast cancer develop resistance to ER-directed agents in the metastatic setting. Beyond mutations in the ER itself, which occur in 25–30% of people treated with aromatase inhibitors[1–4], knowledge about clinical resistance mechanisms remains incomplete. We identified activating HER2 mutations in metastatic biopsies from eight patients with ER+ metastatic breast cancer who had developed resistance to aromatase inhibitors, tamoxifen or fulvestrant. Examination of treatment-naive primary tumors in five patients showed no evidence of pre-existing mutations in four of five patients, suggesting that these mutations were acquired under the selective pressure of ER-directed therapy. The HER2 mutations and ER mutations were mutually exclusive, suggesting a distinct mechanism of acquired resistance to ER-directed therapies. In vitro analysis confirmed that the HER2 mutations conferred estrogen independence as well as—in contrast to ER mutations—resistance to tamoxifen, fulvestrant and the CDK4 and CDK6 inhibitor palbociclib. Resistance was overcome by combining ER-directed therapy with the irreversible HER2 kinase inhibitor neratinib.

The epidermal growth factor receptor 2 (*ERBB2*, which encodes HER2) is frequently altered in cancer; in breast cancer this is manifested primarily via gene amplification[5] or HER2 overexpression. There is considerable in vitro evidence that HER2 signaling may have a complementary role to the estrogen pathway in estrogen receptor–positive (ER+) breast cancer, through ER cross-talk or downstream signaling to provide survival signals in the context of estrogen deprivation[6–13] (see Supplementary Note). Mutations in HER2 are comparatively rare in breast cancer, accounting for 1.6% of primary breast cancers in The Cancer Genome Atlas study[14]. Several activating hotspot mutations in the kinase and extracellular domains have been characterized[14–17]. However, the role of such mutations in metastatic breast cancer (MBC) is less well understood.

As part of an ongoing sequencing study of ER+ MBC[18], we performed whole-exome sequencing (WES) of metastatic tumor biopsies from 168 patients, nearly all of whom had received prior endocrine therapy[18]. In 12 patients, we identified mutations in *ERBB2*, including hotspot mutations in the kinase domain, as well as in the extracellular, transmembrane, and cytoplasmic domains (Fig. 1a). The kinase domain mutants HER2 p.Leu755Ser, p.Val777Leu, and p.Leu869Arg have previously been identified and characterized as activating in breast cancer[14,15]. The transmembrane domain alteration p.Ser653Cys (homologous to the activating epidermal growth factor receptor (EGFR) alteration p.Ser645Cys[19,20]) has not been described in breast cancer, although it was previously observed in one patient with urothelial bladder carcinoma, where it was characterized as activating and sensitive to lapatinib[21]. One metastatic biopsy had both p.Gly727Ala and p.Val777Leu alterations; this combination has been reported in breast cancer[22], and homologous alterations to p.Gly727Ala are activating in EGFR (Gly719)[23] and found in combination with other EGFR mutations in non-small cell lung cancer[24]. The extracellular domain and cytoplasmic domain mutants have not been previously reported. Overall, the increased prevalence of HER2 alterations in the metastatic setting seen here (compared to primary ER+ breast cancer[5,25,26]) is consistent with recent sequencing studies that included MBC[27–31] (Supplementary Fig. 1 and Supplementary Table 1), though those studies did not specifically discuss HER2 alterations in MBC.

To determine whether these 12 HER2 alterations were acquired in the metastatic setting, we obtained and performed WES on corresponding primary tumor biopsies collected before exposure to any endocrine therapy in eight patients[18]. In six of the eight primary tumors (75%), the HER2 alterations identified in the metastatic biopsies were not observed, suggesting that these alterations were acquired over the course of therapy (Fig. 1a, red triangles).

Among eight patients with activating HER2 alterations in their metastatic biopsies (Fig. 1b), the activating HER2 alterations were found to be acquired in four patients, shared in one, and indeterminate in three. All patients were treated with ER-directed therapy before their metastatic biopsies, including tamoxifen (five patients),

[1]Center for Cancer Precision Medicine, Dana-Farber Cancer Institute, Boston, MA, USA. [2]Department of Medical Oncology, Dana-Farber Cancer Institute, Boston, MA, USA. [3]Harvard Medical School, Boston, MA, USA. [4]Broad Institute of MIT and Harvard, Cambridge, MA, USA. [5]Klarman Cell Observatory, Broad Institute of MIT and Harvard, Cambridge, MA, USA. [6]Department of Medicine, Brigham and Women's Hospital, Boston, MA, USA. [7]Division of Oncology, Department of Medicine, Siteman Cancer Center, Washington University School of Medicine, St. Louis, MO, USA. [8]Howard Hughes Medical Institute and Koch Institute of Integrative Cancer Research, Department of Biology, Massachusetts Institute of Technology, Cambridge, MA, USA. [9]These authors contributed equally: U. Nayar, O. Cohen. *e-mail: nikhil_wagle@dfci.harvard.edu

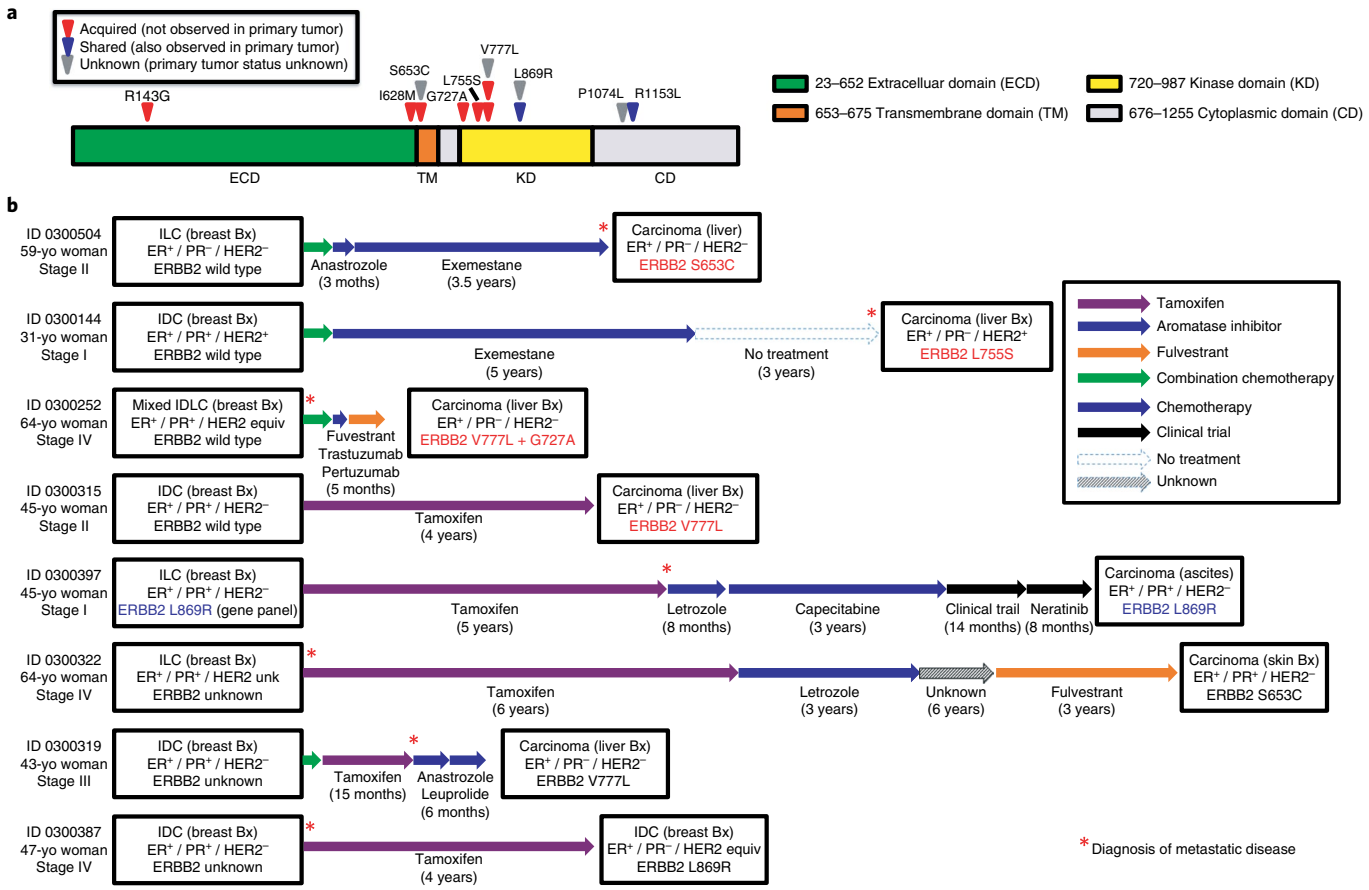

Fig. 1 | Acquired HER2 alterations in patients with endocrine resistance. a, The location of HER2 alterations identified by sequencing metastatic biopsies is depicted along the length of the protein. Protein domains are indicated by color coding. Evolutionary classification for alterations: red triangles, acquired alterations; blue triangles, alterations shared with primary tumor; grey triangles, indeterminate or unknown. **b**, Clinical timelines for the eight ER+ MBC patient bearing HER2 alterations in metastatic biopsies. Patient histories are shown from breast cancer diagnosis until metastatic biopsy sequenced in this study; arrows represent distinct therapies and durations, described in legend. In each case, asterisks demarcate the time that metastatic disease was diagnosed. yo, years old; Bx, biopsy; PR, progesterone receptor; equiv, equivalent; unk, unknown.

aromatase inhibitors (six patients) and fulvestrant (two patients). For the four patients with uncharacterized HER2 alterations, two were acquired, one shared, and one indeterminate (Supplementary Fig. 2). Additional alterations were observed in 593 cancer genes in metastatic biopsies and corresponding primary tumors (Fig. 2a). Detailed clinicopathological features, therapies, and genomic data for all patients and samples are in Supplementary Tables 2–6.

To further explore the role of acquired HER2 alterations in these tumors, we performed an evolutionary analysis to evaluate clonal structure and dynamics. We evaluated the change in the estimated fraction of tumor cells harboring each genomic alteration (the cancer cell fraction, CCF) from the pretreatment primary biopsy to the resistant metastatic biopsy (Fig. 2b). In all four patients, HER2 alterations were not detected in the primary tumor, despite power to detect alterations at this locus (Supplementary Table 5). In three of the metastatic biopsies, the activating HER2 alterations were clonally acquired. In the fourth biopsy, the HER2 alteration was subclonal, although evaluation of the clonality was confounded by a concurrent HER2 amplification. Other alterations, including known driver alterations, were clonal in both primary and metastasis in these patients. Evolutionary analysis for patients with uncharacterized HER2 alterations is in Supplementary Fig. 3.

Although *ESR1* mutations are an established mechanism of resistance to aromatase inhibitors in ER+ MBC[1–4], none of the patients with acquired HER2 alterations had *ESR1* mutations in their metastatic biopsies, suggesting that these might be mutually exclusive events. Examination of publicly available sequencing data from the American Association for Cancer Research (AACR) Project GENIE database V1.0.1 (ref. [30]) showed that *ERBB2* and *ESR1* mutations were indeed mutually exclusive, consistent with our results. Of 1,019 MBC samples (ER+ and ER–), 48 samples had an *ERBB2* mutation only, 109 had an *ESR1* mutation only, and one had both mutations (odds ratio = 0.17, $P = 0.0269$, one-sided Fisher's exact test). Based on these findings, along with the higher overall incidence of acquired activating HER2 alterations in our cohort, we hypothesized that HER2 alterations are a mechanism of acquired resistance to ER-directed therapy in ER+ MBC.

To investigate whether acquired HER2 alterations directly confer resistance to ER-directed therapy, we acutely expressed all HER2 mutant proteins observed in the 12 patients in the ER+ HER2 breast cancer cell lines T47D and MCF7 through lentiviral transduction and examined the impact of acute infection on susceptibility to endocrine agents. These included estrogen deprivation (using charcoal-dextran-stripped serum medium), which recapitulates aromatase inhibitor treatment in vitro, tamoxifen, and the selective estrogen receptor degraders fulvestrant and GDC-0810 (ref. [32]). As controls, we transduced cells with wild-type HER2 and the kinase-dead HER2 mutant p.Asp845Ala[16].

T47D cells expressing alterations in the kinase domain (p.Leu755Ser, p.Val777Leu and p.Leu869Arg) or transmembrane

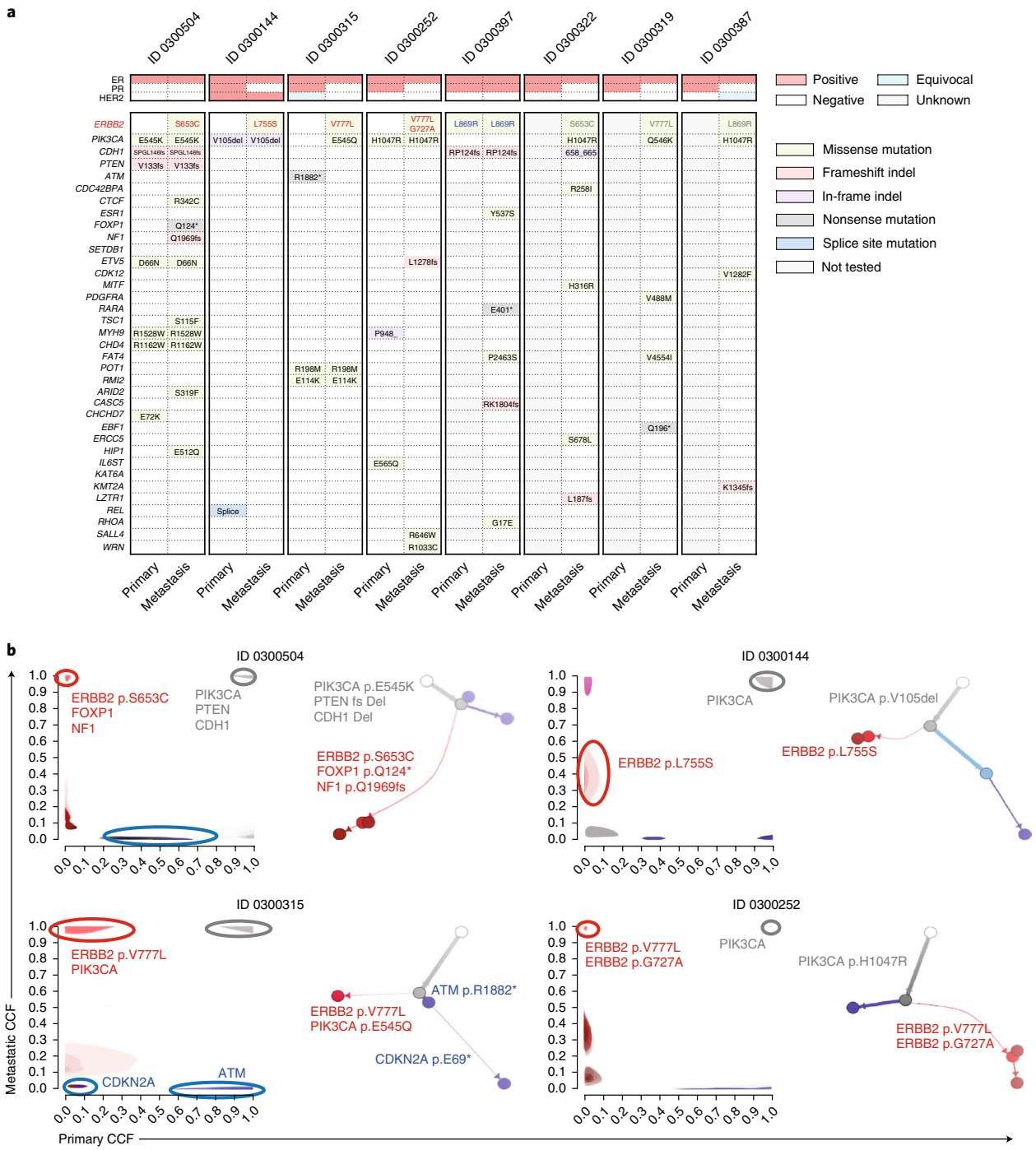

Fig. 2 | Alterational landscape, clonal structure and evolutionary dynamics in HER2 mutant metastatic tumors and matched primary tumors. **a**, Single-nucleotide variants and small insertions or deletions (indels) are depicted across the eight metastatic tumors with activating ERBB2 alterations (top row) and, when available, matched primary tumors. All nonsilent alterations in coding regions of the protein with high clonality (CCF >50%) for 593 cancer genes are shown. The primary tumor for patient 0300397 was sequenced using a targeted gene panel[43–45], so for genes not included in this panel the alterational status is unknown (grey). For patient 0300322, the CDH1 alteration leads to p.658_665LEVGDYKI>F (the annotation is truncated in the figure). Clinical tracks annotate each sample by their ER status, progesterone receptor status and HER2 status. **b**, The clonal dynamics are shown for four metastatic samples with activating HER2 alterations by comparing the metastatic CCF (*y*-axis) to the matched primary CCF (*x*-axis). HER2 alterations are mapped to metastatic acquired clones in all four patients (in red, top left corner), not detected in the primary tumor, and found as clonal in the metastatic tumor in three patients (p.Ser653Cys, p.Val777Leu, p.[Val777Leu]+[Gly727Ala]) and subclonal in one patient (p.Leu755Ser). 'Truncal' alterations that are shared between the metastatic and the primary tumors are found in all patients, demonstrating that the primary and metastatic samples are clonally related (in grey, top right corner, CCF ~1 in both the primary and the metastatic samples). Primary-specific alterations are found in clones that were dominant in the primary but these clones are not observed in the metastatic tumor (in blue). The phylogenetic relationships among clones are reconstructed for each patient starting from the normal cell (white circle) connected to the ancestral cancer cells (grey trunk). The phylogenetic divergence to the primary clones (and subclones) is depicted with blue edges, and phylogenetic divergence to the metastatic clones (and subclones) is in red. Selected mutations in cancer genes are marked on the corresponding branches of the cancer phylogeny.

domain (p.Ser653Cys) were strongly resistant to estrogen deprivation in vitro, conferring a level of resistance equivalent to the previously described resistance-associated *ESR1* ligand-binding domain alteration p.Tyr537Ser (Fig. 3a). Wild-type HER2 conferred only modest resistance, and the kinase-dead p.Asp845Ala alteration[16] did not alter sensitivity as compared to green fluorescent protein (GFP)-expressing cells. We obtained similar results in MCF7 cells (Supplementary Fig. 4a).

Although *ESR1* ligand-binding domain mutations confer robust resistance to estrogen deprivation, they confer only partial resistance to tamoxifen and fulvestrant[1–4]. In contrast, HER2 kinase domain and transmembrane domain mutants were completely resistant to tamoxifen (Fig. 3b), fulvestrant (Fig. 3c) and GDC-0810 (Fig. 3d). Similar results were observed in MCF7 cells (Supplementary Fig. 4). Wild-type HER2 as well as extracellular domain and cytoplasmic domain mutants conferred intermediate resistance between that of ESR1 p.Tyr537Ser and the kinase domain and transmembrane domain mutants (Fig. 3b–d and Supplementary Figs. 4–6). Expression levels of HER2 were similar for all HER2 constructs (Fig. 3e,f). Expressing the p.[Gly727Ala]+[Val777Leu] kinase domain alteration (observed in patient 0300252) conferred resistance to all ER-directed therapies (Supplementary Fig. 7). All in vitro drug sensitivities were consistent with clinical resistance phenotypes in patients bearing the respective HER2 alterations (Fig. 1b). Similar findings were seen at low levels of mutant HER2 expression, by using HER2 mutants expressed under a tetracycline-responsive promoter in cells grown in low doses of doxycycline (Supplementary Fig. 8).

HER2 activates pro-survival signaling pathways in cells, including RAS/RAF/MAPK and PI3K/AKT. HER2 mutants were associated with hyperphosphorylation of both ERK and AKT under conditions of estrogen deprivation or inhibition (Fig. 3e,f). ESR1 p.Tyr537Ser did not hyperactivate MAPK or AKT signaling, whereas extracellular domain and cytoplasmic domain mutants had effects similar to wild-type HER2 (Supplementary Fig. 5e,f). HER2 mutant cells also had lower levels of ER than controls (Fig. 3e), consistent with prior studies in tamoxifen-resistant cells that also showed lower levels of ER[33]. Treatment with fulvestrant led to an additional decrease of ER in HER2 mutant cells, but did not affect AKT or ERK phosphorylation (Fig. 3f).

To investigate whether ER signaling is suppressed in HER2 mutant cells, we examined transcript levels of *ESR1* and the ER targets progesterone receptor (*PGR*), *GREB1* and *TFF1* by quantitative PCR with reverse transcription (qRT-PCR). *ESR1* transcript levels were significantly downregulated in HER2 mutant cells along with *PGR* and *GREB1* (Fig. 3g), although *TFF1* was upregulated. The downregulation of *PGR* was consistent with the phenotype observed in the metastatic biopsies from patients, where acquisition of activating HER2 alterations coincided with loss of progesterone receptor expression by immunohistochemistry (Figs. 1b and 2). The extracellular domain and cytoplasmic domain HER2 mutants suppressed ER, progesterone receptor and GREB1 only slightly (Supplementary Fig. 5g).

To further examine transcriptional changes associated with HER2 mutants, we performed RNA sequencing on cells expressing the four activating HER2 mutants as well as GFP, wild-type HER2, kinase-dead HER2, and ESR1 p.Tyr537Ser, which were all treated with either dimethylsulfoxide (DMSO) or fulvestrant (Fig. 4a). Principal component analysis of the transcriptomes showed that the four HER2 activating mutants clustered together and remained separate from a cluster containing cells expressing ESR1 p.Tyr573Ser, as well as from a cluster containing cells expressing GFP and kinase-dead HER2, and one containing wild-type HER2 (Fig. 4b). Under treatment with fulvestrant, 5,293 genes were significantly differentially expressed (q value = 0.01) between cells expressing the activating HER2 mutants and GFP (Fig. 4c and Supplementary Tables 7 and 8). We next defined a shared HER2-MUT expression signature across the four activating HER2 mutants. Gene set enrichment analysis[34] showed that the shared signature is enriched for *ERBB1* and *ERBB2* signaling and RAS/MAPK signaling compared to GFP and wild-type HER2 cells treated with fulvestrant or DMSO (Fig. 4d, panels 1 and 2; Supplementary Tables 9–12).

Canonical ER targets were among both the upregulated and downregulated HER2-MUT genes (Fig. 4d, panel 3), consistent with our quantitative RT-PCR of *PGR*, *GREB1* and *TFF1* (Fig. 3g). We hypothesized that HER2 mutants may lead to reprogrammed ER signaling, similar to the previously described growth factor–induced ER cistrome[35]. Indeed, the HER2-MUT signature was significantly enriched for induction of growth factor–induced ER targets in HER2 mutant cells (Fig. 4d, panel 4), along with a concomitant suppression of targets induced by estradiol, as previously observed in tamoxifen-resistant MCF7 cells[33]. Individually, all four HER2 mutants demonstrated the elevated RAS/MAPK transcriptional signature (Fig. 4e) as well as the *ERBB1* and *ERBB2* signatures and growth factor–driven ER signatures (Supplementary Fig. 9).

HER2 kinase domain alterations activate HER2 signaling through conformational changes to the catalytic domain that destabilize the inactive conformation of the kinase[14] (Fig. 5a). The p.Gly727Ala and p.Val777Leu co-alterations are in apposition as indicated, and probably modify kinase domain conformation and sensitivity to reversible kinase inhibitors, as shown for EGFR previously[36]. In contrast, the mechanism of activation of the p.Ser653Cys transmembrane domain alteration has not been reported (Fig. 5b). We hypothesized that the cysteine residues form disulfide bridges, leading to constitutive HER2 homodimerization. To test this, we performed immunoblotting under nonreducing conditions to look for intact HER2 dimers. HER2 p.Ser653Cys but none of the other mutants we tested showed higher-molecular-mass species, indicating reduction-sensitive dimers (Fig. 5c). Thus, p.Ser653Cys probably functions by constitutive dimerization, as has been observed for HER2 extracellular domain mutants p.Gly309Glu and p.Glu321Gly[16] as well as other transmembrane domain mutants[37,38] (Fig. 5d).

Neratinib, an irreversible kinase inhibitor with anti-pan-HER activity, inhibits HER2 p.Leu755Ser, p.Val777Leu, and p.Leu869Arg in vitro[14,15] and has shown promise in monotherapy clinical trials in breast cancer patients with activating HER2 alterations[39,40]. Low doses of neratinib resensitized HER2 mutant cells to fulvestrant (Fig. 6a). These cells were also sensitive to neratinib monotherapy at a higher dose (Supplementary Fig. 10c). In all cases, combination with fulvestrant inhibited viability better than neratinib alone, suggesting that inhibition of HER2 mutants restored sensitivity to fulvestrant. In contrast, neratinib only partially resensitized ESR1 p.Tyr537Ser cells to fulvestrant (Fig. 6a,b), and high-dose neratinib monotherapy was also ineffective in these cells (Supplementary Fig. 10a,c and Supplementary Note).

Neratinib treatment of HER2 mutant cells decreased both ERK and AKT phosphorylation (Fig. 6b and Supplementary Fig. 10b). In contrast, pharmacologic inhibition of individual downstream effectors MEK, ERK, PI3K, AKT and MTOR, alone or in combination with fulvestrant, did not restore sensitivity to fulvestrant in HER2 mutant cells (Supplementary Fig. 10e,f).

Combination treatment with endocrine therapy and CDK4 and CDK6 inhibitors is currently a standard-of-care treatment for ER$^+$ MBC. HER2 mutant cells were cross-resistant to the CDK4 and CDK6 inhibitor palbociclib, both alone and in combination with fulvestrant (Fig. 6c and Supplementary Fig. 10d). Consistent with this, RNA sequencing (RNA-seq) analysis showed that HER2 mutant cells treated with palbociclib, either as single agent or with fulvestrant, grouped with DMSO- and fulvestrant-treated cells; cells treated with neratinib, with or without fulvestrant, grouped separately (Fig. 6d). RAS/MAPK transcriptional activity remained robust in the presence of palbociclib monotherapy or combination

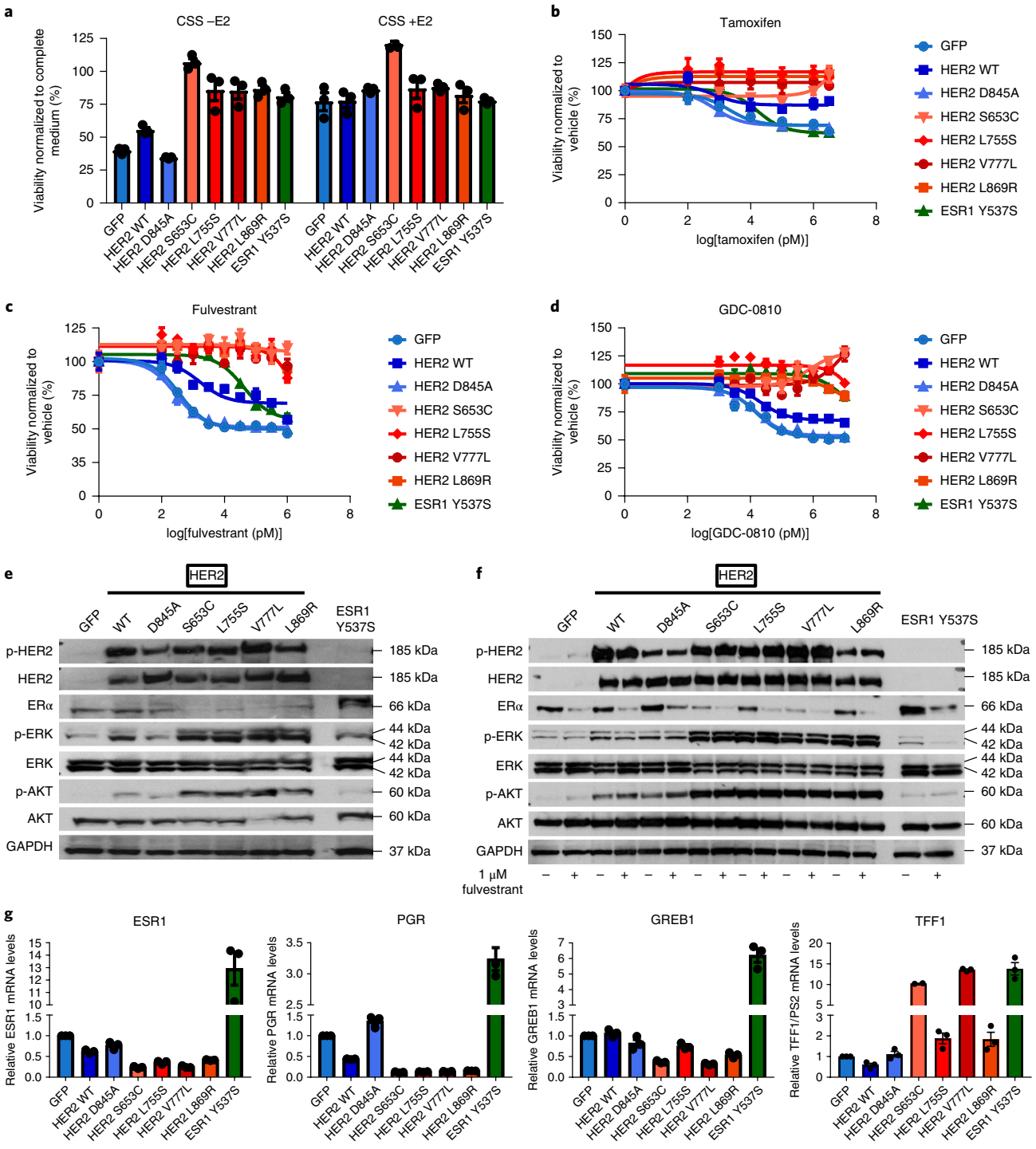

Fig. 3 | HER2 alterations confer endocrine resistance. a–d, T47D HER2 mutant and control cells were compared on the basis of sensitivity to estrogen deprivation and anti-ER agents tamoxifen, fulvestrant and GDC-0810. **a**, T47D cells expressing the indicated HER2 mutants or controls were serum-starved for 2 d, followed by treatment with vehicle or 10 nM estradiol (E2), as indicated. After a week, relative viability compared to cells grown in complete media was analyzed by CellTiter-Glo. Results shown are mean ± s.e.m. of three technical replicates, and representative of 14 independent experiments. **b–d**, Cells were plated as in **a**, and switched to full medium containing a range of concentrations of tamoxifen (**b**), fulvestrant (**c**) or GDC-0810 (**d**) after 2 d. Cells were re-treated after 3 d. Viability was determined by CellTiter-Glo assay after a week, and normalized to untreated wells. Results shown are mean ± s.e.m. and representative of 13, 15 or 9 independent experiments, respectively. **e**,**f**, Levels of HER2 activation markers phospho-ERK (p-ERK) and phospho-AKT (p-AKT) were examined by western blotting in T47D HER2 mutant and control cells. T47D HER2 mutant and control cells were plated in estrogen-deprived medium for 48 h, then switched to fresh medium supplemented with CSS (**e**), or complete medium containing DMSO or 1 μM fulvestrant (**f**), for 24 h. Whole-cell extracts were analyzed by western blotting using the indicated antibodies. Results shown are representative of six and two independent experiments, respectively. **g**, Levels of ER downstream target transcripts were examined by qPCR in T47D HER2 mutant and control cells. T47D HER2 mutant and control cells were plated in estrogen-deprived medium for 48 h, followed by RNA extraction and quantitative RT-PCR using primers for ESR1, PGR, GREB1 or TFF1 as indicated. Results shown are mean ± s.e.m. of three independent experiments.

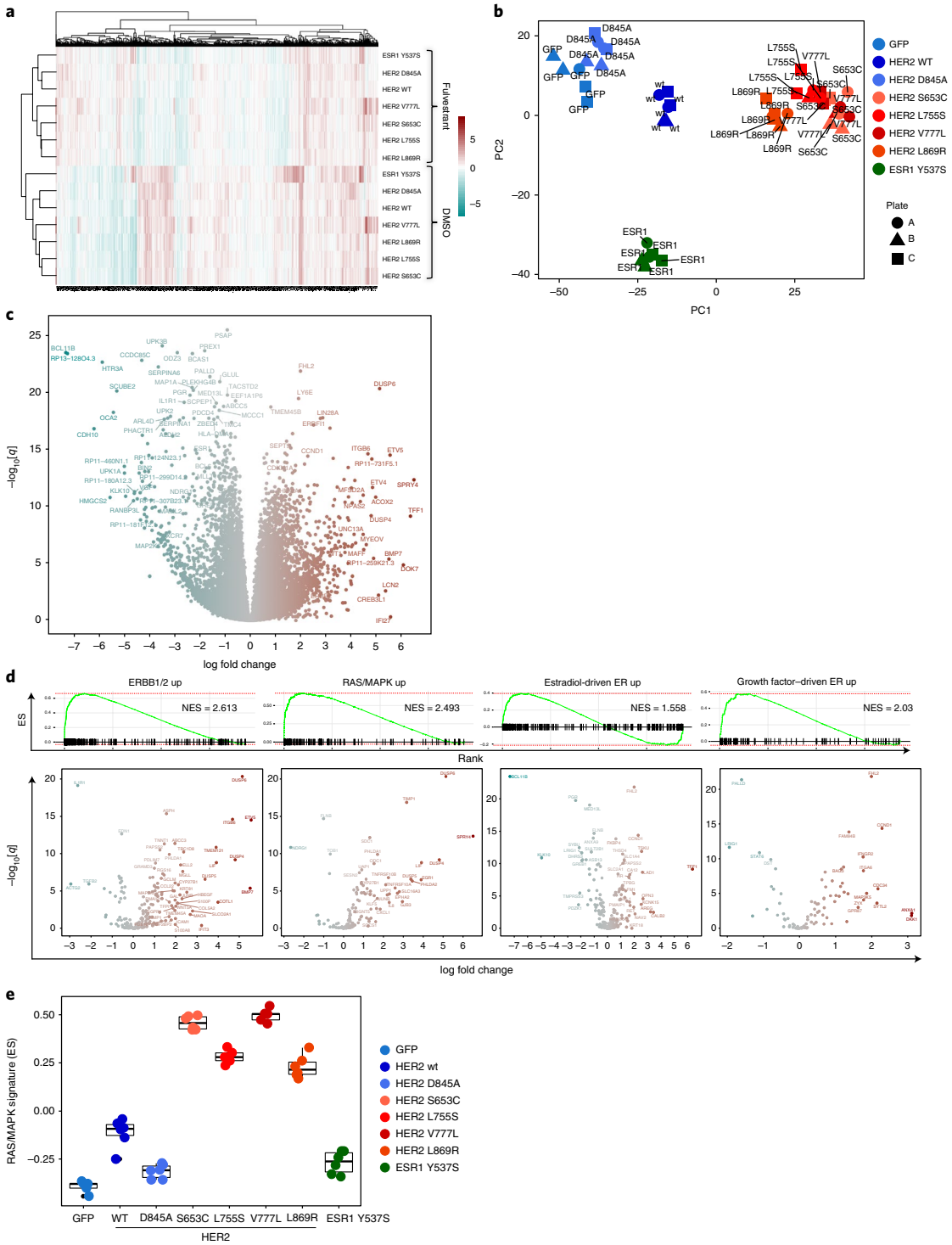

Fig. 4 | Transcriptional cell-state analysis of HER2 mutant cells. Gene expression analysis by RNA sequencing of T47D cells expressing the indicated mutants or controls was performed after 2 d of serum starvation followed by treatment with DMSO or 1 μM fulvestrant for 24 h. Six replicates were performed for each specific construct and drug condition (with at least five passing quality control). **a**, Unsupervised hierarchical clustering of HER2 activating mutants, wild-type HER2, kinase-dead HER2 p.Asp845Ala, and ESR1 p.Tyr537Ser transcriptomes treated with either DMSO or fulvestrant. **b**, Principal component analysis of all biological replicates of HER2 mutants and controls under treatment with fulvestrant. PC, principal component. **c**, DEGs contrasting all HER2 activating mutants (p.Ser653Cys, p.Leu755Ser, p.Val777Leu and p.Leu869Arg) with GFP, under treatment with fulvestrant. DEGs with the highest magnitude (by log-fold change) and significance are labeled. **d**, Using DEGs between all HER2 activating mutants and GFP under treatment with fulvestrant, a common transcriptional footprint for the HER2 mutants was inferred, termed HER2-MUT. Gene set enrichment analysis was performed using HER2-MUT and showed significant enrichment in signatures representing growth factor–induced gene expression[46] (ERBB1/2 up) and MAPK signaling[47] (RAS/MAPK up). A mixed profile was observed for the canonical (estradiol-driven) ER signature[46] (estradiol-driven ER up); however, a highly enriched profile was found for a growth factor–driven ER signature[35] (growth factor–driven ER up). NES, normalized enrichment score; ES, enrichment score. **e**, The RAS/MAPK signature strength is shown for each of the HER2 mutants and the controls, across all replicates, in cells treated with fulvestrant.

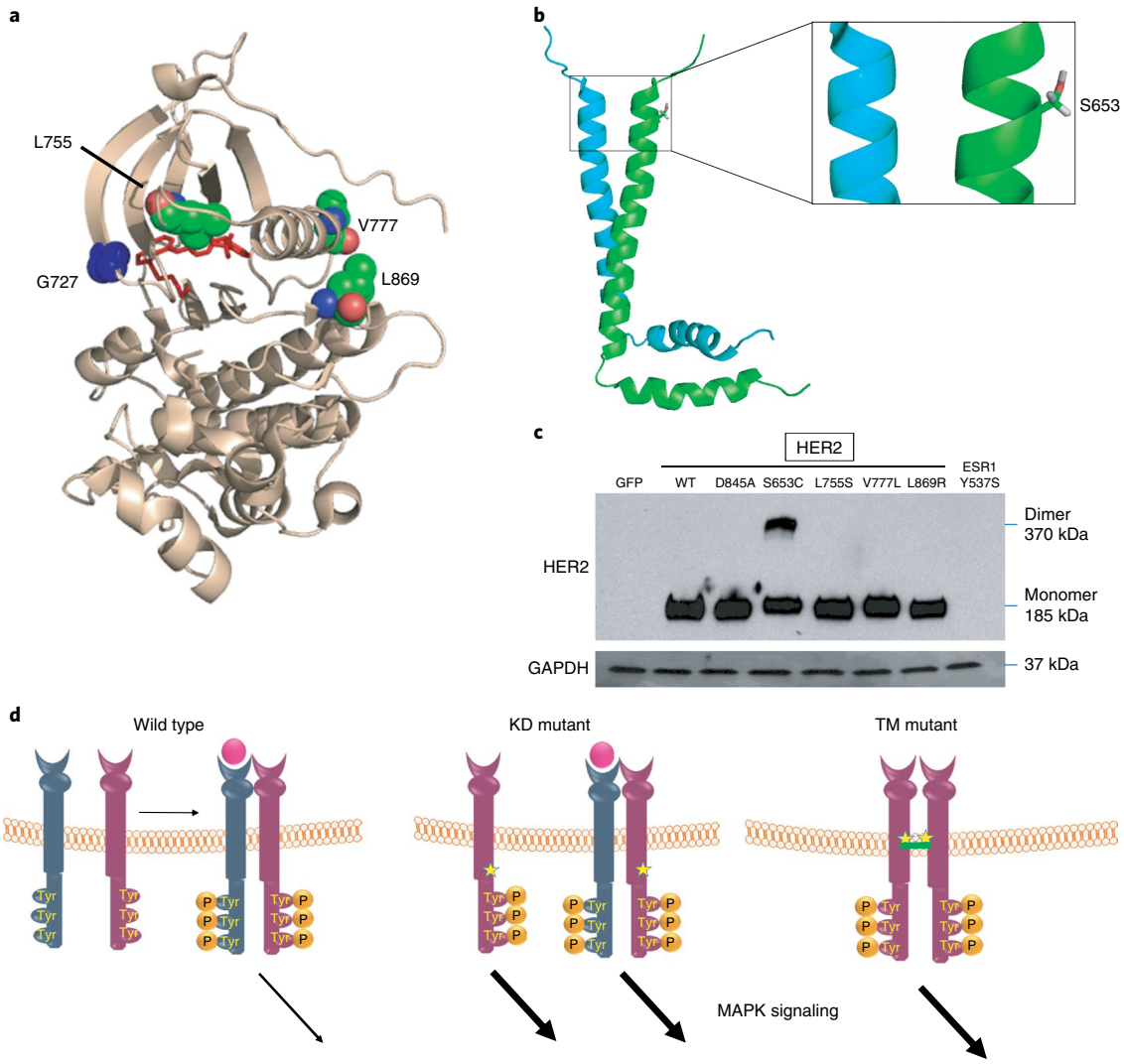

Fig. 5 | Mechanism of activation of HER2 mutants. a, Structure of the HER2 active kinase domain (PDB entry 3PP0) bound to a reversible kinase inhibitor (red molecule), with the locations of the kinase domain alterations identified in the patients in this study indicated. p.Leu755Ser and p.Leu869Arg probably disrupt a cluster of hydrophobic residues that stabilize the inactive conformation of the molecule as in the case of EGFR[48]. In addition to activation by this mechanism, p.Val777Leu and the p.[Gly727Ala]+[Val777Leu] alterations probably affect the ability of HER2 to bind reversible kinase inhibitors as described for Gly719 in EGFR[36]. **b**, Structure of the HER2 transmembrane domain (PDB entry 2N2A) with the location of the identified transmembrane domain mutant p.Ser653Cys. The cysteine residue may form intermolecular disulfide bridges with other mutant HER2 monomers. **c**, T47D HER2 mutant cells were examined for the presence of reduction-sensitive HER2 dimers, as a marker of constitutive disulfide bridge formation. T47D wild-type HER2 or mutant HER2 cells plated in complete medium were extracted using nonreducing buffer containing iodoacetamide. Extracts were prepared and run under nonreducing conditions and then probed with antibodies to HER2. The location of the HER2 monomer and dimers, as determined by expected molecular mass, is indicated. GAPDH was used as a loading control. Results shown are representative of three independent experiments. KD, kinase domain; TD, transmembrane domain. **d**, A hypothetical model for hyperactive MAPK signaling arising from the HER2 mutants is depicted. Left: in cells bearing wild-type HER2, HER2 monomers (blue) heterodimerize with other ERBB monomers (EGFR or HER3, purple) bound to their cognate ligand (pink), leading to C-terminal tail phosphorylation and signaling. Middle: HER2 bearing kinase domain alterations are in a constitutively active conformation and possibly hyperautophosphorylated and capable of signaling as described previously for other kinase domain alterations in HER2 (ref. [49]) and EGFR[50]. When these monomers heterodimerize with other members of the HER family such as EGFR or HER3 (blue) that are bound to their cognate ligand (pink), transphosphorylation leads to enhanced heterodimer signaling. kinase domain mutants may also homodimerize as previously shown for wild-type HER2 overexpression (not depicted). Right: HER2 transmembrane domain mutants probably form intermolecular disulfide bridges with other HER2 monomers bearing the alteration, which would enable phosphorylation and activation in a ligand-independent manner.

therapy (Fig. 6e). However, neratinib treatment, both as a single agent and with fulvestrant, led to repression of RAS/MAPK transcriptional activity (Fig. 6e) and other transcriptional effects of HER2 mutants (Supplementary Fig. 11). This was borne out clinically in one patient in the cohort with an acquired HER2 p.Val777Leu alteration after developing disease progression while on treatment with tamoxifen, who had intrinsic resistance to subsequent letrozole and palbociclib therapy (Fig. 6f). The discovery of the acquired HER2 alteration in the metastatic biopsy prompted enrollment of the patient into a phase 2 trial of fulvestrant plus neratinib[41], resulting in a partial response lasting 6 months, consistent with our in vitro findings (Fig. 6a).

Taken together, our results suggest that activating HER2 alterations are a distinct mechanism of acquired resistance to multiple

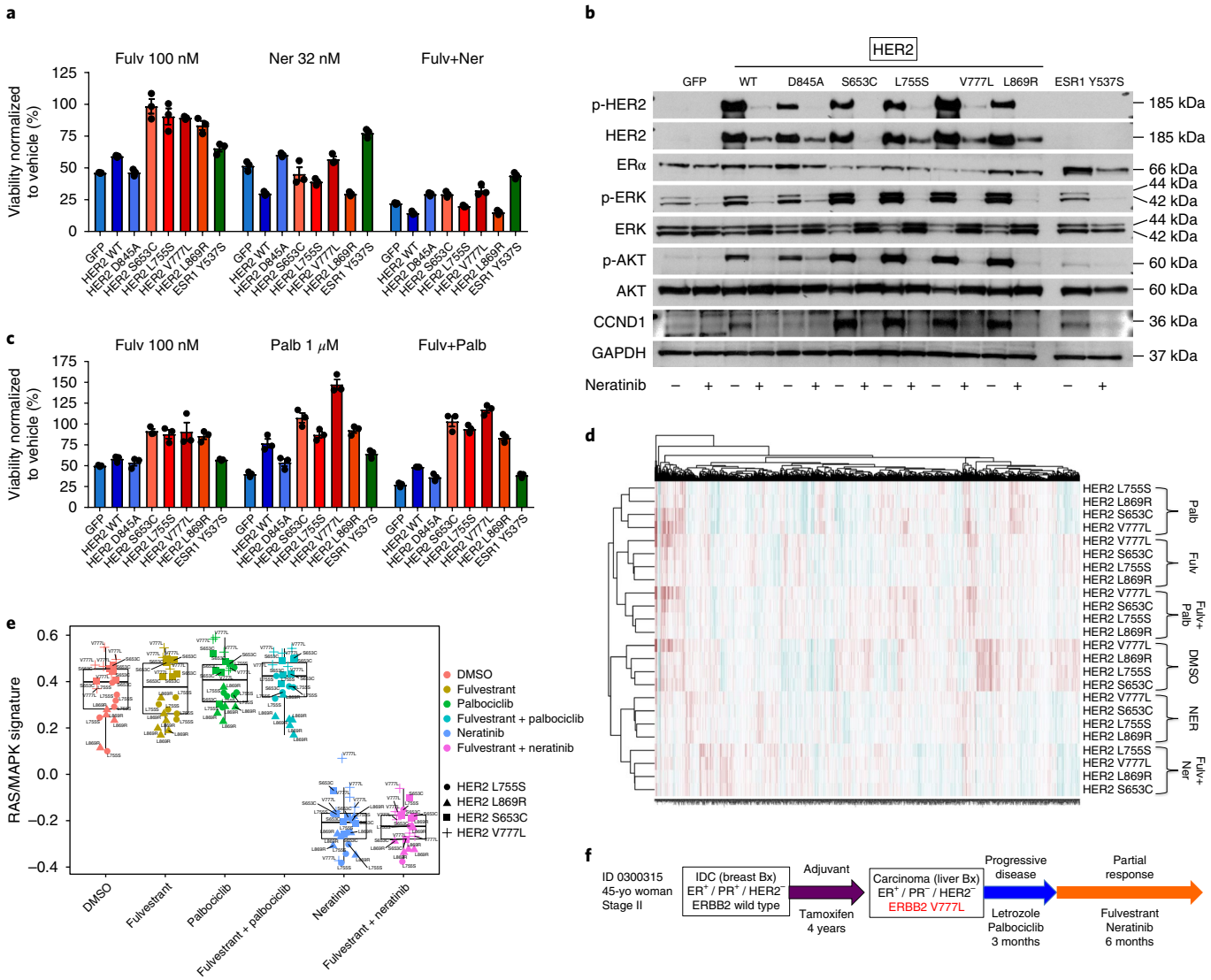

Fig. 6 | ER+ cells with HER2 alterations are sensitive to fulvestrant plus neratinib. a, T47D HER2 mutant and control cells were compared on the basis of sensitivity to pan-HER kinase inhibitor neratinib (Ner) alone or in combination with fulvestrant (Fulv). T47D HER2 mutant and control cells serum-starved for 2 d were switched to complete medium containing 100 nM fulvestrant, 32 nM neratinib or a combination of the two. Cells were re-treated after 3 d, and viability was determined by CellTiter-Glo assay 1 week after the start of treatment. Results shown are mean ± s.e.m., and representative of 14 independent experiments. **b**, Levels of HER2 activation markers phospho-ERK and phospho-AKT were examined by western blotting in T47D HER2 mutant and control cells treated with neratinib. T47D HER2mut and control cells serum starved for 48 h were switched to complete medium containing DMSO or 1 μM neratinib for 24 h. Whole-cell extracts were analyzed for the indicated proteins by immunoblotting. Results shown are representative of three independent experiments. **c**, The response to the CDK4 and CDK6 inhibitor palbociclib (Palb) was examined in T47D HER2 mutant and control cells, both alone and in combination with fulvestrant. Cells plated as in **a** were treated with 100 nM fulvestrant, 1 μM palbociclib, or a combination of both. Results shown are mean ± s.e.m. and representative of five independent experiments. **d**,**e**, Gene expression analysis by RNA sequencing performed as described in Fig. 4 included T47D cells expressing the four activating HER2 mutants, GFP, wild-type HER2, kinase-dead HER2 or ESR1 Tyr537Ser, as indicated. Cells were serum-starved then treated with 1 μM fulvestrant, 1 μM neratinib, 10 μM palbociclib or combinations (1 μM fulvestrant + 1 μM neratinib; 1 μM fulvestrant + 10 μM palbociclib). Six replicates were performed for each specific construct and drug condition, for a total of 288 transcriptomes (8 constructs × 6 drug conditions × 6 replicates). **d**, Unsupervised hierarchical clustering of the cells bearing the four activating HER2 mutants treated with DMSO, fulvestrant, neratinib, palbociclib, fulvestrant + neratinib or fulvestrant + palbociclib. **e**, The RAS/MAPK signature strength was compared in mutant cell lines under various treatment conditions. **f**, Treatment history of an endocrine-resistant patient with an acquired p.Val777Leu alteration showed intrinsic resistance to the combination of palbociclib and letrozole, and subsequent partial response to the combination of fulvestrant and neratinib.

forms of ER-directed therapy in MBC that can be overcome by an irreversible HER2 inhibitor. Our observations also suggest that, with the increasing clinical use of selective estrogen receptor degraders, which can overcome *ESR1* mutations, the prevalence of HER2 alterations might increase. The acquisition of targetable activating alterations in the metastatic setting highlights the importance of serial profiling of metastatic tumor biopsies or cell-free DNA from blood at the time of resistance in people with ER+ MBC. Identification of HER2 alterations in real time may help identify patients who will not benefit from ER-directed therapies or should be directed to clinical trials testing strategies to overcome this mechanism of resistance. One such strategy, the combination of fulvestrant and neratinib, is

being tested in phase 2 clinical trials[42] with promising preliminary results reported in individual patients[15] including within our cohort (Fig. 6f). Ultimately, the use of upfront combinations to preempt the emergence of HER2-mutant-resistant clones may lead to more durable responses in people with ER+ MBC.

URLs. Gene Expression Omnibus (GEO), https://www.ncbi.nlm.nih.gov/geo/; Database of Genotypes and Phenotypes (dbGAP), https://www.ncbi.nlm.nih.gov/gap; Picard, http://picard.sourceforge.net/; Firehose, http://www.broadinstitute.org/cancer/cga/Firehose; Indelocator, http://www.broadinstitute.org/cancer/cga/indelocator; MuTect2, https://software.broadinstitute.org/gatk/documentation/tooldocs/current/org_broadinstitute_gatk_tools_walkers_cancer_m2_MuTect2; Novoalign, www.novocraft.com/products/novoalign/; ReCapSeg, http://gatkforums.broadinstitute.org/categories/recapseg-documentation; Oncotator, http://www.broadinstitute.org/cancer/cga/oncotator; CCF and evolutionary analysis, https://software.broadinstitute.org/cancer/cga/absolute.

Online content

Any methods, additional references, Nature Research reporting summaries, source data, statements of data availability and associated accession codes are available at https://doi.org/10.1038/s41588-018-0287-5.

Received: 30 October 2017; Accepted: 23 October 2018;
Published online: 10 December 2018

References

1. Merenbakh-Lamin, K. et al. D538G mutation in estrogen receptor-alpha: A novel mechanism for acquired endocrine resistance in breast cancer. *Cancer Res.* **73**, 6856–6864 (2013).
2. Robinson, D. R. et al. Activating ESR1 mutations in hormone-resistant metastatic breast cancer. *Nat. Genet.* **45**, 1446–1451 (2013).
3. Toy, W. et al. ESR1 ligand-binding domain mutations in hormone-resistant breast cancer. *Nat. Genet.* **45**, 1439–1445 (2013).
4. Jeselsohn, R. et al. Emergence of constitutively active estrogen receptor-alpha mutations in pretreated advanced estrogen receptor-positive breast cancer. *Clin. Cancer Res.* **20**, 1757–1767 (2014).
5. Cancer Genome Atlas Network. Comprehensive molecular portraits of human breast tumours. *Nature* **490**, 61–70 (2012).
6. Giuliano, M., Trivedi, M. V. & Schiff, R. Bidirectional crosstalk between the estrogen receptor and human epidermal growth factor receptor 2 signaling pathways in breast cancer: molecular basis and clinical implications. *Breast Care (Basel)* **8**, 256–262 (2013).
7. Osborne, C. K. & Schiff, R. Mechanisms of endocrine resistance in breast cancer. *Annu. Rev. Med.* **62**, 233–247 (2011).
8. Hurtado, A. et al. Regulation of ERBB2 by oestrogen receptor-PAX2 determines response to tamoxifen. *Nature* **456**, 663–666 (2008).
9. Liu, S. et al. Targeting tyrosine-kinases and estrogen receptor abrogates resistance to endocrine therapy in breast cancer. *Oncotarget* **5**, 9049–9064 (2014).
10. Knowlden, J. M. et al. Elevated levels of epidermal growth factor receptor/c-erbB2 heterodimers mediate an autocrine growth regulatory pathway in tamoxifen-resistant MCF-7 cells. *Endocrinology* **144**, 1032–1044 (2003).
11. Frogne, T. et al. Activation of ErbB3, EGFR and Erk is essential for growth of human breast cancer cell lines with acquired resistance to fulvestrant. *Breast Cancer Res. Treat.* **114**, 263–275 (2009).
12. Benz, C. C. et al. Estrogen-dependent, tamoxifen-resistant tumorigenic growth of MCF-7 cells transfected with HER2/neu. *Breast Cancer Res. Treat.* **24**, 85–95 (1992).
13. Elledge, R. M. et al. HER-2 expression and response to tamoxifen in estrogen receptor-positive breast cancer: a Southwest Oncology Group study. *Clin. Cancer Res.* **4**, 7–12 (1998).
14. Bose, R. et al. Activating HER2 mutations in HER2 gene amplification negative breast cancer. *Cancer Discov.* **3**, 224–237 (2013).
15. Hanker, A. B. et al. An acquired HER2 T798I gatekeeper mutation induces resistance to neratinib in a patient with HER2 mutant-driven breast cancer. *Cancer Discov.* **7**, 575––585 (2017).
16. Greulich, H. et al. Functional analysis of receptor tyrosine kinase mutations in lung cancer identifies oncogenic extracellular domain mutations of ERBB2. *Proc. Natl Acad. Sci. USA* **109**, 14476–14481 (2012).
17. Zabransky, D. J. et al. HER2 missense mutations have distinct effects on oncogenic signaling and migration. *Proc. Natl Acad. Sci. USA* **112**, E6205–E6214 (2015).
18. Cohen, O. et al. Abstract S1-01: Whole exome and transcriptome sequencing of resistant ER+ metastatic breast cancer. *Cancer Res.* **77**, S1-01–S1-01 (2017).
19. Imielinski, M. et al. Mapping the hallmarks of lung adenocarcinoma with massively parallel sequencing. *Cell* **150**, 1107–1120 (2012).
20. Berger, A. H. et al. High-throughput phenotyping of lung cancer somatic mutations. *Cancer Cell* **30**, 214–228 (2016).
21. de Martino, M. et al. Impact of ERBB2 mutations on in vitro sensitivity of bladder cancer to lapatinib. *Cancer Biol. Ther.* **15**, 1239–1247 (2014).
22. Pereira, B. et al. The somatic mutation profiles of 2,433 breast cancers refines their genomic and transcriptomic landscapes. *Nat. Commun.* **7**, 11479 (2016).
23. Yun, C. H. et al. Structures of lung cancer-derived EGFR mutants and inhibitor complexes: mechanism of activation and insights into differential inhibitor sensitivity. *Cancer Cell* **11**, 217–227 (2007).
24. Kobayashi, S. et al. Compound EGFR mutations and response to EGFR tyrosine kinase inhibitors. *J. Thorac. Oncol.* **8**, 45–51 (2013).
25. Curtis, C. et al. The genomic and transcriptomic architecture of 2,000 breast tumours reveals novel subgroups. *Nature* **486**, 346–352 (2012).
26. Ciriello, G. et al. Comprehensive molecular portraits of invasive lobular breast cancer. *Cancer Cell* **163**, 506–519 (2015).
27. Lefebvre, C. et al. Mutational profile of metastatic breast cancers: a retrospective analysis. *PLoS Med.* **13**, e1002201 (2016).
28. Yates, L. R. et al. Genomic evolution of breast cancer metastasis and relapse. *Cancer Cell* **32**, 169–184.e7 (2017).
29. Zehir, A. et al. Mutational landscape of metastatic cancer revealed from prospective clinical sequencing of 10,000 patients. *Nat. Med.* **23**, 703–713 (2017).
30. AACR Project GENIE Consortium. AACR Project GENIE: powering precision medicine through an international consortium. *Cancer Discov.* **7**, 818–831 (2017).
31. Robinson, D. R. et al. Integrative clinical genomics of metastatic cancer. *Nature* **548**, 297–303 (2017).
32. Lai, A. et al. Identification of gdc-0810 (arn-810), an orally bioavailable selective estrogen receptor degrader (serd) that demonstrates robust activity in tamoxifen-resistant breast cancer xenografts. *J. Med. Chem.* **58**, 4888–4904 (2015).
33. Massarweh, S. et al. Tamoxifen resistance in breast tumors is driven by growth factor receptor signaling with repression of classic estrogen receptor genomic function. *Cancer Res.* **68**, 826–833 (2008).
34. Sergushichev, A. An algorithm for fast preranked gene set enrichment analysis using cumulative statistic calculation. Preprint at https://www.biorxiv.org/content/early/2016/06/20/060012 (2016).
35. Lupien, M. et al. Growth factor stimulation induces a distinct ER(alpha) cistrome underlying breast cancer endocrine resistance. *Genes Dev.* **24**, 2219–2227 (2010).
36. Jiang, J. et al. Epidermal growth factor-independent transformation of Ba/F3 cells with cancer-derived epidermal growth factor receptor mutants induces gefitinib-sensitive cell cycle progression. *Cancer Res.* **65**, 8968–8974 (2005).
37. Burke, C. L., Lemmon, M. A., Coren, B. A., Engelman, D. M. & Stern, D. F. Dimerization of the p185neu transmembrane domain is necessary but not sufficient for transformation. *Oncogene* **14**, 687–696 (1997).
38. Chen, L. I., Webster, M. K., Meyer, A. N. & Donoghue, D. J. Transmembrane domain sequence requirements for activation of the p185c-neu receptor tyrosine kinase. *J. Cell. Biol.* **137**, 619–631 (1997).
39. Ma, C. X. et al. Neratinib efficacy and circulating tumor DNA detection of HER2 mutations in HER2 nonamplified metastatic breast cancer. *Clin. Cancer Res.* **23**, 5687–5695 (2017).
40. Hyman, D. M. et al. HER kinase inhibition in patients with HER2- and HER3-mutant cancers. *Nature* **554**, 189–194 (2018).
41. Ma, C. X. B. R. et al. Phase II trial of neratinib for HER2 mutated, non-amplified metastatic breast cancer (HER2mut MBC). *J. Clin. Oncol.* **34**, abstr 516 (2016).
42. Hyman, D. et al. Abstract PD2-08: Neratinib + fulvestrant in ERBB2-mutant, HER2–non-amplified, estrogen receptor (ER)-positive, metastatic breast cancer (MBC): Preliminary analysis from the phase II SUMMIT trial. *Cancer Res.* **77**, https://doi.org/10.1158/1538-7445.SABCS16-PD2-08 (2017).
43. Wagle, N. et al. High-throughput detection of actionable genomic alterations in clinical tumor samples by targeted, massively parallel sequencing. *Cancer Discov.* **2**, 82–93 (2012).
44. MacConaill, L. E. et al. Prospective enterprise-level molecular genotyping of a cohort of cancer patients. *J. Mol. Diagn.* **16**, 660–672 (2014).
45. Sholl, L. M. et al. Institutional implementation of clinical tumor profiling on an unselected cancer population. *JCI Insight* **1**, e87062 (2016).
46. Liberzon, A. et al. The molecular signatures database (MSigDB) hallmark gene set collection. *Cell Syst.* **1**, 417–425 (2015).
47. Bild, A. H. et al. Oncogenic pathway signatures in human cancers as a guide to targeted therapies. *Nature* **439**, 353–357 (2006).
48. He, M. et al. EGFR exon 19 insertions: a new family of sensitizing EGFR mutations in lung adenocarcinoma. *Clin. Cancer Res.* **18**, 1790–1797 (2012).

49. Wang, S. E. et al. HER2 kinase domain mutation results in constitutive phosphorylation and activation of HER2 and EGFR and resistance to EGFR tyrosine kinase inhibitors. *Cancer Cell* **10**, 25–38 (2006).
50. Kancha, R. K., von Bubnoff, N., Peschel, C. & Duyster, J. Functional analysis of epidermal growth factor receptor (EGFR) mutations and potential implications for EGFR targeted therapy. *Clin. Cancer Res.* **15**, 460–467 (2009).

Acknowledgements

We thank Q. Quartey and P. Ram for technical assistance, F. Luo, R. Jeselsohn, C. Strathdee, I. Leshchiner, D. Rosebrock, D. Livitz and G. Getz for technical advice, and B. Kaplan, H. Greulich, C. Strathdee, F. Luo, E. Goetz and L. Garraway for providing reagents. We thank C. Johannessen, M. Brown, M. Meyerson and R. Bose for helpful discussions and comments on the manuscript. We are grateful to all the patients who volunteered for our tumor biopsy protocol and generously provided the tissue analyzed in this study. This work was supported by the Department of Defense W81XWH-13-1-0032 (N.W.), AACR Landon Foundation 13-60-27-WAGL (N.W.), National Cancer Institute Breast Cancer SPORE at DF/HCC P50CA168504 (N.W.), Susan G. Komen CCR15333343 (N.W.), the V Foundation (N.W.), the Breast Cancer Alliance (N.W.), the Cancer Couch Foundation (N.W.), the MBC Collective (N.W.), Breast Cancer Research Foundation (N.U.L. and E.P.W.), ACT NOW (to Dana-Farber Cancer Institute Breast Oncology Program), Fashion Footwear Association of New York (to Dana-Farber Cancer Institute Breast Oncology Program), Friends of Dana-Farber Cancer Institute (to N.U.L.), the Klarman Family Foundation and HHMI (to A.R.) and Dana-Farber/Harvard Cancer Center SPORE grant P50CA168504.

Author contributions

U.N., O.C. and N.W. conceived and designed the study; U.N., C.K. and M.S.C. performed experiments; O.C. performed the computational analyses; O.C. and S.F. evaluated the evolutionary trajectories; A.G.W., S.A.W. and N.W. performed clinical data abstraction and annotation; C.P. and N.S.P. performed kinase structural modeling; O.R. and A.R. supervised the RNA-seq experiment; L.M., K.H. and N.O. assisted with acquisition and annotation of clinical samples; C.X.M. is the principal investigator on the clinical trial of fulvestrant/neratinib on which patient 315 was treated; E.P.W., N.U.L. and N.W. oversaw patient enrollment and sample collection on the metastatic biopsy protocol; U.N., O.C. and N.W. wrote the manuscript with input from all authors; N.W. supervised the study.

Competing interests

N.W. was previously a stockholder in Foundation Medicine, was previously a consultant for Novartis, and has received sponsored research support from Novartis and Puma Biotechnology. N.U.L. has received research funding from Genentech, Cascadian Therapeutics, Array Biopharma, Novartis and Pfizer. C.X.M. receives consulting fees from Puma Biotechnology, Novartis and Pfizer, and research funding from Puma Biotechnology and Pfizer. S.A.W. is a consultant for Foundation Medicine and InfiniteMD. E.P.W. is a consultant for InfiniteMD, Genentech and Eli Lilly. A.R. is a scientific advisory board member of ThermoFisher Scientific, Syros Pharmaceuticals and Driver Group and a founder of Celsius Therapeutics. None of these entities had any role in the conceptualization, design, data collection, analysis, decision to publish or preparation of the manuscript.

Additional information

Supplementary information is available for this paper at https://doi.org/10.1038/s41588-018-0287-5.

Reprints and permissions information is available at www.nature.com/reprints.

Correspondence and requests for materials should be addressed to N.W.

Publisher's note: Springer Nature remains neutral with regard to jurisdictional claims in published maps and institutional affiliations.

Methods

Patient and tumor samples. Before any study procedures, all patients provided written informed consent for research biopsies and whole-exome sequencing of tumor and normal DNA, as approved by the Dana-Farber/Harvard Cancer Center Institutional Review Board (DF/HCC Protocol 05-246). Metastatic core biopsies were obtained from patients and samples were immediately snap frozen in optimal cutting temperature compound (OCT) and stored at −80 °C. Archival formalin-fixed, paraffin-embedded (FFPE) blocks of primary tumor samples were also obtained. A blood sample was obtained during the course of treatment, and whole blood was stored at −80 °C until DNA extraction was performed.

Whole-exome sequencing. DNA was extracted from primary tumors, metastatic tumors and normal samples for all patients and whole-exome sequencing was performed as detailed below.

DNA extraction. DNA extraction was performed as described[51]. For whole blood, DNA was extracted using magnetic bead–based chemistry in conjunction with the Chemagic MSM I instrument manufactured by Perkin Elmer. After red blood cell lysis, magnetic beads bound to the DNA and were removed from solution using electromagnetized rods. Several wash steps followed to eliminate cell debris and protein residue from DNA bound to the magnetic beads. DNA was then eluted in Tris-EDTA buffer. For frozen tumor tissue, DNA and RNA were extracted simultaneously from a single frozen tissue or cell pellet sample using the AllPrep DNA/RNA kit (Qiagen). For FFPE tumor tissues, DNA and RNA were extracted simultaneously using Qiagen's AllPrep DNA/RNA FFPE kit. All DNA was quantified using Picogreen.

Library construction. DNA libraries for massively parallel sequencing were generated as described[51] with the following modifications: the initial genomic DNA input into the shearing step was reduced from 3 µg to 10–100 ng in 50 µl of solution. For adapter ligation, Illumina paired-end adapters were replaced with palindromic forked adapters (purchased from Integrated DNA Technologies) with unique dual indexed 8-base index molecular barcode sequences included in the adapter sequence to facilitate downstream pooling. With the exception of the palindromic forked adapters, all reagents used for end repair, A-base addition, adapter ligation and library enrichment PCR were purchased from KAPA Biosciences in 96-reaction kits. In addition, during the post-enrichment solid-phase reversible immobilization (SPRI) bead cleanup, elution volume was reduced to 30 µl to maximize library concentration, and a vortexing step was added to maximize the amount of template eluted.

Solution-phase hybrid selection. After library construction, hybridization and capture were performed using the relevant components of Illumina's Rapid Capture Exome Kit and according to the manufacturer's suggested protocol, with the following exceptions: first, all libraries within a library construction plate were pooled before hybridization. Second, the Midi plate from Illumina's Rapid Capture Exome kit was replaced with a skirted PCR plate to facilitate automation. All hybridization and capture steps were automated on the Agilent Bravo liquid handling system.

Preparation of libraries for cluster amplification and sequencing. After post-capture enrichment, library pools were quantified using quantitative PCR (qPCR, KAPA Biosystems) with probes specific to the ends of the adapters; this assay was automated using Agilent's Bravo liquid handling platform. Based on qPCR quantification, libraries were normalized and denatured using 0.1 N NaOH on the Hamilton Starlet.

Cluster amplification and sequencing. Cluster amplification of denatured templates was performed according to the manufacturer's protocol (Illumina) using HiSeq 2500 Rapid Run v1/v2, HiSeq 2500 High Output v4 or HiSeq 4000 v1 cluster chemistry and HiSeq 2500 (Rapid or High Output) or HiSeq 4000 flowcells. Flowcells were sequenced on HiSeq 2500 using v1 (Rapid Run flowcells) or v4 (High Output flowcells) Sequencing-by-Synthesis chemistry or v1 Sequencing-by-Synthesis chemistry for HiSeq 4000 flowcells. The flowcells were then analyzed using RTA v.1.18.64 or later. Each pool of whole-exome libraries was run on paired 76 base pair runs, with two 8-base index sequencing reads to identify molecular indices, across the number of lanes needed to meet coverage for all libraries in the pool.

Sequence data processing. Exome sequence data processing was performed using established analytical pipelines at the Broad Institute. A BAM file was produced with the Picard pipeline (see URLs), which aligns the tumor and normal sequences to the hg19 human genome build using Illumina sequencing reads. The BAM was uploaded into the Firehose pipeline (see URLs), which manages input and output files to be executed by GenePattern[52].

Sequencing quality control. Quality control modules within Firehose were applied to all sequencing data for comparison of the origin for tumor and normal genotypes and to assess fingerprinting concordance. Cross-contamination of samples was estimated using ContEst[53].

Somatic alteration assessment. MuTect[54] was applied to identify somatic single-nucleotide variants. Indelocator (see URLs), Strelka[55], and MuTect2 (see URLs) were applied to identify small insertions or deletions. A voting scheme was used for inferred indels that required scoring by at least two of three algorithms.

Artifacts introduced by DNA oxidation (so-called OxoG) during sequencing were computationally removed using a filter-based method[56]. In the analysis of primary tumors that are FFPE samples we further applied a filter to remove FFPE-related artifacts[57].

Reads around mutated sites were realigned with Novoalign (see URLs) to filter out false-positive results that are due to regions of low reliability in the reads alignment. At the last step, we filtered mutations that are present in a comprehensive WES panel of 8,334 normal samples (using the Agilent technology for WES capture), aiming to filter either germline sites or recurrent artifactual sites. We further used a smaller WES panel of 355 normal samples that are based on Illumina technology for WES capture, and another panel of 140 normal samples sequenced without our cohort[18] to further capture possible batch-specific artifacts. Annotation of identified variants was done using Oncotator[58] (see URLs).

Copy number and copy ratio analysis. To infer somatic copy number from WES, we used ReCapSeg (see URLs), calculating proportional coverage for each target region (that is, number of reads in the target divided by total number of reads) followed by segment normalization using the median coverage in a panel of normal samples. The resulting copy ratios were segmented using the circular binary segmentation algorithm[59].

To infer allele-specific copy ratios, we mapped all germline heterozygous sites in the germline normal sample using GATK Haplotype Caller[60] and then evaluated the read counts at the germline heterozygous sites to assess the copy profile of each homologous chromosome. The allele-specific copy profiles were segmented to produce allele-specific copy ratios.

Cancer cell fraction and evolutionary analysis. *Analysis using ABSOLUTE.* To properly compare single-nucleotide variants and indels in paired metastatic and primary samples, we considered the union of all mutations called in either of the two samples. We evaluated the reference and alternate reads in each patient's primary and metastatic tumors, including mutations that were not initially called in one of the samples. These mutations in matched samples were used as input for ABSOLUTE[61]. The ABSOLUTE algorithm uses mutation-specific variant allele fractions together with the computed purity, ploidy and segment-specific allelic copy ratio to compute CCFs.

Analysis of clonal dynamics using PHYLOGIC. To evaluate the mutation clonality in the patient-matched primary and metastatic samples, we used PHYLOGIC clustering of the mutation-specific CCFs as described[62,63]. The CCF of indels may be systematically underestimated owing to counting of only a subset of the reads supporting the indel event in cases of longer indels. For example, CCF was underestimated in the CDH1, c.437_447delCTCCTGGCCTC indel in patient 300504 in both metastatic and primary samples, but upon re-evaluation of the BAM files and supporting reads we assigned this mutation to the shared truncal mutations (clonal in both primary and metastatic samples). Further details regarding CCF and evolutionary analysis are online (see URLs).

Selected cancer genes (mutational landscape of potential drivers). The list of mutated genes (Fig. 2) include: (1) significantly mutated genes in breast cancer[64] or significantly mutated genes in our metastatic cohort[18], including *ERBB2*, *PIK3CA*, *CDH1*, *PTEN*, *ATM*, *CDC42BPA*, *CTCF*, *ESR1*, *FOXP1*, *NF1* and *SETDB1*; (2) genes with plausible clinical impact[57] including *ETV5*, *CDK12*, *MITF*, *PDGFRA*, *RARA* and *TSC1*; and (3) genes from Cancer Gene Census, COSMIC database v82 (ref. [65]), including *MYH9*, *CHD4*, *FAT4*, *POT1*, *RMI2*, *ARID2*, *CASC5*, *CHCHD7*, *EBF1*, *ERCC5*, *HIP1*, *IL6ST*, *KAT6A*, *KMT2A*, *LZTR1*, *REL*, *RHOA*, *SALL4* and *WRN*.

Cell culture. ER$^+$ HER2 T47D (American Type Culture Collection (ATCC), HTB-133) and MCF7 cells (ATCC, HTB-22) were cultured in phenol red–free RPMI-1640 (Gibco, 11835-030) or phenol red–free MEMα (Gibco, 41061-029) supplemented with 10% FBS (Gemini, 100-106), respectively. HEK293T/17 (ATCC, CRL-11268) cells were cultured in DMEM (Gibco, 11995-065) supplemented with 10% FBS. For serum starvation conditions, the appropriate medium was supplemented with 10% charcoal-dextran-stripped serum (Gemini, 100-119).

Generation of HER2 mutant plasmids and cells. HER2 mutants were generated by site-directed mutagenesis of the *ERBB2* open reading frame in a pDONR223 vector backbone, using the QuikChange II site-directed mutagenesis kit (Agilent Technologies, 200523). After sequencing, the mutant constructs were cloned into the pLX307 vector backbone or the pDEST40 vector using the gateway LR clonase kit (Life Technologies, 11791019) to facilitate generation of mutant-encoding lentivirus, as described below.

To generate HER2 mutant or control lentivirus, 293T cells were transfected to produce viral particles using FuGENE HD (Promega, E2311) with VSV-G and

Δ8.91 envelope and packaging plasmids. After 72 h of incubation the supernatant was filtered through a 0.45-μm filter (Corning, 431225), tested for the presence of lentiviral particles using Lenti-x GoStix (Takara, 631244) and stored at −80 °C until transduction. Lentiviral transduction of T47D cells plated in 6-well dishes was accomplished by viral spinoculation of cells in medium containing 4 μg ml^{-1} polybrene (Santa Cruz, sc-134220). After overnight incubation, medium was replaced. The cells were selected in 1.5 μg ml^{-1} puromycin (Gibco, A11138-03) 48 h after infection for 2 d, after which medium was replaced with fresh medium containing puromycin, and selected for a further 2 d. After confirmation of complete selection in uninfected control wells, cells were trypsinized, counted and plated for viability, western blotting, qPCR or HER2 dimerization assays as described below.

In cases in which estrogen deprivation was required, cells were cultured in phenol red–free RPMI containing 10% charcoal-dextran-stripped FBS (Gemini, 100-119) after selection.

HER2 inducible cell lines. To generate HER2 inducible cell lines, pDONR223 constructs encoding various HER2 mutants or controls, as well as pDONR223-GFP and pDONR223-HER2 wild type, were cloned into the Gateway-compatible pLX403 vector, which drives transgene expression using a Tet-On system.

The pLX317-GFP and pLX317-HER2 controls and pDONR223-HER2 plasmid were obtained from the Broad Institute The RNAi Consortium (TRC) portal. The VSV-G envelope and Δ8.91 packaging plasmids, pLX307 Gateway cloning destination vector and pLX403 vector were gifts from Levi Garraway (Dana-Farber Cancer Institute). Lentivirus encoding all mutants and controls was generated as described above, followed by transfection into T47D cells and bulk selection with puromycin to generate a stable cell line in each case. The cells were treated with various concentrations of doxycycline (Clontech, 631311) ranging from 25 to 500 ng ml^{-1}, for various time periods ranging from 3 h to 1 week, to determine the minimal dose and induction time of doxycycline required to stimulate HER2 mutant expression over endogenous levels. Transgene expression was seen as early as 3 h after induction at 25 ng ml^{-1} doxycycline.

Kill curves. T47D HER2 mutant cells were plated in RPMI with 10% charcoal dextran-stripped serum (CSS) at 1,000 cells per well of 96-well Viewplates (Perkin-Elmer, 6005181). After 2 d of serum starvation, cells were switched over to complete medium or treated with estradiol (Sigma-Aldrich, E2758) as appropriate, and treated with a range of doses of the corresponding drug. Cells were re-treated after 3 d. One week after the start of treatment, viability was determined using CellTiter-Glo as described below. The normalized data were plotted in GraphPad Prism, and analyzed by nonlinear regression curve fit using the log (inhibitor) versus response three-parameter model.

CellTiter-Glo viability assays. One week after the start of treatment, the medium in 96-well plates was replaced with 100 μl fresh medium per well and brought to room temperature. CellTiter-Glo (Promega, G7572) was added to each well (20 μl), lysed for 2 min at ~250 r.p.m. and then equilibrated at room temperature for 20 min. A plate reader was programmed to integrate luminescence for 500 ms per well. Background luminescence from medium-only wells was subtracted from all values, and raw values were normalized against untreated wells for each cell line.

Chemicals and antibodies. Chemicals used included iodoacetamide (Sigma-Aldrich, A3221-10V), fulvestrant (Sigma-Aldrich, I4409-25mg), neratinib (Selleck Chemicals, S2150), (Z)-4-hydroxyTamoxifen (Sigma-Aldrich, H7904-25mg), GDC-0810 (Medkoo, 206041), AZD5363 (Thermo Fisher Scientific, NC0488926), VX-11e (Selleck Chemicals, S7709), trametinib (GSK1120212, Selleck Chemicals, S2673), BYL719 (Selleck Chemicals, S2814), RAD001/everolimus (Selleck Chemicals, S1120) and palbociclib (Selleck Chemicals, S1116). Primary antibodies used included antibodies to p-HER2 (EMD Millipore, 06-229), HER2 (Cell Signaling Technology, clone 44E7, 2248S), ERα (Santa Cruz Biotechnology, clone HC-20, SC-543), p-ERK1 and p-ERK2 (CST, clone E10, 9106S), ERK1 and ERK2 (CST, clone 137F5, 4695S), p-AKT (CST, clone D9W9U, 12694S), AKT (CST, 9272S), CCND1 (CST, clone 92G2, 2978), GAPDH (SCB, clone V-18, SC-20357) and β-actin (Santa Cruz, 47778), as well as goat anti-rabbit (Pierce, 32260), rabbit anti-goat (Invitrogen, 81-1620) and goat anti-mouse (Novex, A16090) antibodies.

Western blotting. About 5.0 × 10^5 HER2 mutant or control cells were serum-starved for 2 d, then treated with 1 μM fulvestrant or 1 μM neratinib for 24 h. Whole-cell protein extracts were made by passive lysis with 50 μl of lysis buffer, comprised of RIPA buffer (Sigma-Aldrich, R0278-50ml), 1 mM DL-dithiothreitol (DTT, Sigma-Aldrich, D0632-5G), 1 mM phenylmethylsulfonyl fluoride (Sigma-Aldrich, P7626-5G), protease inhibitor (Sigma-Aldrich, P8340-5ml), and Halt phosphatase inhibitor (Thermo Fisher Scientific, 78428). Cell pellets were lysed on a rotator at 15 r.p.m. for 15 min at 4 °C; lysates were then cleared by centrifugation at 14,000*g* for 15 min at 4 °C.

Protein was quantified by bicinchoninic acid assay (BCA, Pierce BCA Protein Assay kit, 23225) according to the manufacturer's microplate procedure. Samples were prepared using 30 μg of protein, Bolt LDS Sample Buffer (Life Technologies, B0007), and DTT, then heated to 70 °C for 10 min according to Novex's NuPAGE Bis-Tris Gel sample preparation recommendations. Samples were run on a Bolt 4–12% Bis-Tris Plus gel (Thermo Fisher Scientific, NW04125BOX) at 200 V for 35 min in 1× Bolt MOPS SDS running buffer (Life Technologies, B0001). Protein was transferred to nitrocellulose membranes using the BioRAD transblot turbo according to the fast-transfer protocol in the Trans-Blot Turbo RTA Transfer kit. Membranes were blocked at room temperature for 1 h in 5% milk in Tris-buffered saline (TBS, Bio-Rad, 170-6435) with 0.1% Tween-20 (Sigma-Aldrich, P9416-100 ml). The membranes were incubated overnight at 4 °C with primary antibody at a 1:1,000 dilution in 1% milk in TBS-Tween (TBS-T). The following day the membranes were washed 3× for 5 min with TBS-T and incubated with secondary antibody at a 1:2,000 dilution in 1% milk in TBS-T for 1 h at room temperature. After washing 4 × 10 min with TBS-T, membranes were treated with Pierce ECL Plus Western Blotting Substrate (Life Technologies, 32132) for 5 min and exposed to autoradiography film (Fisher Scientific, NC9648989). Full scans of all western blots in main and supplementary figures are in Supplementary Data.

Quantitative PCR with reverse transcription. About 8.0 × 10^5 T47D HER2 mutant or control cells were serum-starved in RPMI-1640 supplemented with 10% CSS for 48 h. Cells were washed with PBS and trypsinized, and cell pellets were collected and washed once with PBS. RNA was harvested using a RNeasy Mini kit (Qiagen 74104) according to the supplied protocol. RNA (1 μg) was reverse transcribed to cDNA on a ProFlex PCR System thermocycler, according to the RNase inhibitor–free protocol in the High-Capacity cDNA Reverse Transcription kit (Applied Biosystems, 4368814) user manual.

The cDNA was diluted eight-fold in double-distilled H_2O and mixed with PowerUp SYBR Green Master Mix (Applied Biosystems, A25742) and appropriate forward and reverse primer pairs specific for ESR1 and selected targets in a 20-μl reaction according to the manufacturers' specifications. The quantification was performed on an Applied Biosystems 7300 Real-Time PCR System. Each sample was run in triplicate and the raw data were analyzed by the $2^{-\Delta\Delta Ct}$ method and normalized to GFP.

Primers were ordered from Integrated DNA Technologies at 25-nm scale and standard purification. Primer sequences are in Supplementary Table 13.

RNA sequencing on HER2 mutant cell lines and controls. *RNA sequencing experimental setup and treatment of cells.* T47D cells were infected de novo with lentivirus encoding HER2 mutants and controls (GFP, wild-type HER2, kinase-dead HER2 and ESR1 p.Tyr537Ser) in the pLX307 plasmid as described above. Upon completion of selection with puromycin, the cells were plated in 96-well plates in RPMI supplemented with 10% CSS for 48 h. Cells were then treated with DMSO, 1 μM fulvestrant, 1 μM neratinib, 10 μM palbociclib, 1 μM fulvestrant + 1 μM neratinib, or 1 μM fulvestrant + 10 μM palbociclib for 241 μg h^{-1}. The cells were washed 3× with ice-cold PBS and lysed with TCL buffer (Qiagen 157013305) containing 1% β-mercaptoethanol (Sigma, M3148), transferred to PCR plates (Qiagen, 951020401), sealed, spun down for 1 min at 3,000 r.p.m. and immediately frozen at −80 °C until RNA extraction. For each specific construct and drug condition we performed six biological replicates, for a total of 288 transcriptomes (8 constructs × 6 drugs × 6 replicates).

RNA sequencing protocol. Plates with cell lysates were thawed and purified with 2.2× RNAClean SPRI beads (Beckman Coulter Genomics). The RNA-captured beads were air dried and processed immediately for RNA secondary structure denaturation (72 °C for 3 min) and cDNA synthesis. We performed SMART-Seq2 as described[66] with minor modifications in the reverse transcription step. We made a 15-μl reaction mix for each PCR and performed ten cycles for cDNA amplification. We used 0.2 ng cDNA of each population and one-eighth of the standard Illumina NexteraXT (Illumina FC-131-1096) reaction volume in both the tagmentation and PCR amplification steps. Uniquely indexed libraries were pooled and sequenced with NextSeq 500 high-output V2 75 cycle kits (Illumina FC-404-2005) and 38 × 38 paired-end reads on an Illumina NextSeq 500 instrument, aggregating three NextSeq runs.

Reads alignments, expression quantification and quality control. Reads were mapped to the human genome (hg19) with STAR aligner[67] (version 2.5.2b) with default parameters against hg19 of the human genome. Transcriptome quality and expression quantification was conducted using RNA-SeQC[68]. Samples with <12,000 unique genes were removed from subsequent analysis, excluding 26 samples and retaining 262 profiles, with a minimum of three replicates for each activating HER2 mutant (median of six and lower quantile of five replicates). Samples passing quality control had a mean of 17,363 detected genes by at least three reads (s.d. = 755) and a mean of 7,060,935 uniquely mapped pairs of reads (s.d. = 1,191,466).

Principal component analysis. The transcripts per million measured expression per gene was log normalized. To correct for batch effects among the three 96-well plates, we used the ComBat algorithm with default parameters[69]. Principal component analysis was performed with the R implementations of the function prcomp as part of the stats package using the default parameters.

Heatmap analysis. The clustering of transcriptional profiles across various drug conditions used genes with high dispersion among samples, as calculated by LogVMR (variance-to-mean ratio, VMR) as implemented in FindVariableGenes function, Seurat R package.

Differential expression analysis. Differential expression analysis was performed over the raw read counts using limma package[70] with voom assessment[70] of counts normalization and while accounting for the among-plates batch effect.

Definition of HER2-MUT signature. The HER2-MUT signature was inferred from the list of differentially expressed genes (DEGs) by comparing the four activating HER2 alterations (p.Val777Leu, p.Ser653Cys, p.Leu869Arg and p.Leu755Ser) with a given control open reading frame under a given drug condition. Supplementary Tables 9 and 10 depict the HER2-MUT signature with DEG between the mutants and GFP under fulvestrant and DMSO, respectively. Supplementary Tables 11 and 12 depict the HER2-MUT signature with DEGs between the mutants and wild-type HER2 under fulvestrant and DMSO, respectively.

Transcriptional signatures analysis. We used fast gene set enrichment analysis[34] with 50,000 permutations and gene set size limited to a minimum of 3 and a maximum of 1,000 genes, respectively. A total set of 5,095 gene sets was analyzed including the c2, c6 and hallmark collections from MSigDB[46] augmented with a breast cancer gene set collection[35,71,72]. Significant gene sets, controlling for a false discovery rate (FDR) of 5%, are in Supplementary Tables 9 and 10 for enrichments of HER2 mutants versus GFP DEGs under treatment with fulvestrant and DMSO, respectively. Significant gene sets, controlling for a FDR of 5%, are in Supplementary Tables 11 and 12 for enrichments of HER2 mutants versus HER2 wild-type DEGs under treatment with fulvestrant and DMSO, respectively. The evaluation of signature strength for single samples was done using gene set variation analysis[73] with default parameters using the $\log_2$-normalized, batch-corrected expression for each sample.

HER2 dimerization assay. The HER2 dimerization assay was performed as described[16]. Briefly, T47D HER2 mutant or control cells were cultured in phenol red–free RPMI-1640 with 10% FBS in six-well plates until nearly confluent (~3–4 d). Cells were washed twice with cold PBS containing 10 mM iodoacetamide (Sigma-Aldrich, A3221) while on ice. Cells were actively lysed with 200 µl of TGP buffer, comprising 50 mM Tris base (Sigma-Aldrich, T1503), 10% glycerol (Sigma-Aldrich, G5516), 1% Triton X-100 (Sigma-Aldrich, T8787), 10 mM iodoacetamide, 1 mM phosphatase inhibitor and 1 mM protease inhibitor, for 20 min at 4 °C. Lysates were cleared by centrifugation and quantified by BCA. The samples were prepared in LDS sample buffer without DTT, and 25 µg was loaded on gels as described in the "Western blotting" section. After transfer, membranes were probed with anti-HER2 and anti-GAPDH for loading control as described above.

Reporting Summary. Further information on research design is available in the Nature Research Reporting Summary linked to this article.

Data availability

Tumor and germline whole-exome sequencing data generated and analyzed for this study have been deposited in the access-controlled public repository dbGaP with accession code phs001285. RNA-seq data are available through GEO under accession GSE121411. Additional data generated in this study, including tumor exome analysis, are available within the paper and in the supplementary information.

References

51. Fisher, S. et al. A scalable, fully automated process for construction of sequence-ready human exome targeted capture libraries. *Genome. Biol.* **12**, R1 (2011).
52. Reich, M. et al. GenePattern 2.0. *Nat. Genet.* **38**, 500–501 (2006).
53. Cibulskis, K. et al. ContEst: estimating cross-contamination of human samples in next-generation sequencing data. *Bioinformatics* **27**, 2601–2602 (2011).
54. Cibulskis, K. et al. Sensitive detection of somatic point mutations in impure and heterogeneous cancer samples. *Nat. Biotechnol.* **31**, 213–219 (2013).
55. Saunders, C. T. et al. Strelka: accurate somatic small-variant calling from sequenced tumor-normal sample pairs. *Bioinformatics* **28**, 1811–1817 (2012).
56. Costello, M. et al. Discovery and characterization of artifactual mutations in deep coverage targeted capture sequencing data due to oxidative DNA damage during sample preparation. *Nucleic Acids Res.* **41**, e67 (2013).
57. Van Allen, E. M. et al. Whole-exome sequencing and clinical interpretation of formalin-fixed, paraffin-embedded tumor samples to guide precision cancer medicine. *Nat. Med.* **20**, 682–688 (2014).
58. Ramos, A. H. et al. Oncotator: cancer variant annotation tool. *Hum. Mutat.* **36**, E2423–E2429 (2015).
59. Olshen, A. B., Venkatraman, E. S., Lucito, R. & Wigler, M. Circular binary segmentation for the analysis of array-based DNA copy number data. *Biostatistics* **5**, 557–572 (2004).
60. DePristo, M. A. et al. A framework for variation discovery and genotyping using next-generation DNA sequencing data. *Nat. Genet.* **43**, 491–498 (2011).
61. Carter, S. L. et al. Absolute quantification of somatic DNA alterations in human cancer. *Nat. Biotechnol.* **30**, 413–421 (2012).
62. Brastianos, P. K. et al. Genomic characterization of brain metastases reveals branched evolution and potential therapeutic targets. *Cancer Discov.* **5**, 1164–1177 (2015).
63. Stachler, M. D. et al. Paired exome analysis of Barrett's esophagus and adenocarcinoma. *Nat. Genet.* **47**, 1047–1055 (2015).
64. Lawrence, M. S. et al. Discovery and saturation analysis of cancer genes across 21 tumour types. *Nature* **505**, 495–501 (2014).
65. Futreal, P. A. et al. A census of human cancer genes. *Nat. Rev. Cancer* **4**, 177–183 (2004).
66. Picelli, S. et al. Smart-seq2 for sensitive full-length transcriptome profiling in single cells. *Nat. Methods* **10**, 1096–1098 (2013).
67. Dobin, A. et al. STAR: ultrafast universal RNA-seq aligner. *Bioinformatics* **29**, 15–21 (2013).
68. DeLuca, D. S. et al. RNA-SeQC: RNA-seq metrics for quality control and process optimization. *Bioinformatics* **28**, 1530–1532 (2012).
69. Leek, J. T., Johnson, W. E., Parker, H. S., Jaffe, A. E. & Storey, J. D. The sva package for removing batch effects and other unwanted variation in high-throughput experiments. *Bioinformatics* **28**, 882–883 (2012).
70. Ritchie, M. E. et al. limma powers differential expression analyses for RNA-sequencing and microarray studies. *Nucleic Acids Res.* **43**, e47 (2015).
71. Stover, D. G. et al. The role of proliferation in determining response to neoadjuvant chemotherapy in breast cancer: a gene expression-based meta-analysis. *Clin. Cancer Res.* **22**, 6039–6050 (2016).
72. Creighton, C. J. et al. Development of resistance to targeted therapies transforms the clinically associated molecular profile subtype of breast tumor xenografts. *Cancer Res.* **68**, 7493–7501 (2008).
73. Hanzelmann, S., Castelo, R. & Guinney, J. GSVA: gene set variation analysis for microarray and RNA-seq data. *BMC Bioinformatics* **14**, 7 (2013).

nature research

Corresponding author(s): Nikhil Wagle, MD

☐ Initial submission ☐ Revised version ☒ Final submission

Life Sciences Reporting Summary

Nature Research wishes to improve the reproducibility of the work that we publish. This form is intended for publication with all accepted life science papers and provides structure for consistency and transparency in reporting. Every life science submission will use this form; some list items might not apply to an individual manuscript, but all fields must be completed for clarity.

For further information on the points included in this form, see Reporting Life Sciences Research. For further information on Nature Research policies, including our data availability policy, see Authors & Referees and the Editorial Policy Checklist.

Experimental design

1. Sample size

Describe how sample size was determined.

As part of an ongoing sequencing study of ER+ metastatic breast cancer, we performed whole exome sequencing (WES) of metastatic tumor biopsies from 168 patients. In 12 patients, we identified mutations in ERBB2. These 12 patients served as the basis for this report. Becuase they were identified by the presence of an ERBB2 mutation in their tumor, no sample size calculation was performed. We do not make any statistical inference around these 12 patients, but rather describe the sequencing results in their tumors as clinically relevant examples of our subsequent experimental findings.

2. Data exclusions

Describe any data exclusions.

No data were excluded

3. Replication

Describe whether the experimental findings were reliably reproduced.

Experimental findings were reliably reproduced consistently, as described in detail in respective figure legends, methods, and supplementary methods.

4. Randomization

Describe how samples/organisms/participants were allocated into experimental groups.

Samples with HER2 mutations for testing were used for the experimental group, with negative controls (GDP, wild-type HER2, and kinase dead HER2) and positive controls (ESR1 ligand binding domain mutant). No randomization was conducted for these in vitro experiments.

5. Blinding

Describe whether the investigators were blinded to group allocation during data collection and/or analysis.

No blinding was conducted for these in vitro experiments, due to the nature of the experiments.

Note: all studies involving animals and/or human research participants must disclose whether blinding and randomization were used.

6. Statistical parameters

For all figures and tables that use statistical methods, confirm that the following items are present in relevant figure legends (or in the Methods section if additional space is needed).

n/a	Confirmed
☐	☒ The exact sample size (*n*) for each experimental group/condition, given as a discrete number and unit of measurement (animals, litters, cultures, etc.)
☐	☒ A description of how samples were collected, noting whether measurements were taken from distinct samples or whether the same sample was measured repeatedly
☐	☒ A statement indicating how many times each experiment was replicated
☐	☒ The statistical test(s) used and whether they are one- or two-sided (note: only common tests should be described solely by name; more complex techniques should be described in the Methods section)
☐	☒ A description of any assumptions or corrections, such as an adjustment for multiple comparisons
☐	☒ The test results (e.g. *P* values) given as exact values whenever possible and with confidence intervals noted
☐	☒ A clear description of statistics including central tendency (e.g. median, mean) and variation (e.g. standard deviation, interquartile range)
☐	☒ Clearly defined error bars

See the web collection on statistics for biologists for further resources and guidance.

Software

Policy information about availability of computer code

7. Software

Describe the software used to analyze the data in this study.

All software and pipelines for genomic analysis is described in detail in Online Methods.

All genomics analysis software and tools used in this study are published and publicly available. Exome BAM files were produced with the Picard pipeline (http://picard.sourceforge.net). Exome analysis was done with the Firehose environment (http://www.broadinstitute.org/cancer/cga/Firehose) with genomics tools available at http://www.broadinstitute.org/cancer/cga. These tools include ConTest, MuTect, Indelocator, Recapseg, Strekla, Mutect2, Novoalign, Oncotator, GATK Haplotype Caller, Absolute, and Phylogic, as detailed in the Online Methods section.

RNA-seq analysis tools are described in detail in Online Methods, and include:
- alignment with STAR aligner [version 2.5.2b]
- batch effect correction donw with ComBat algorithm (sva R package)
- principal component analysis (PCA) with the R implementations of the function prcomp() as part of the "stats" package
- high dispersion genes using "Seurat" R package (FindVariableGenes function)
- differential expression analysis with limma package with voom assessment
- gene signatures with Fast Gene Set Enrichment Analysis (https://bioconductor.org/packages/release/bioc/html/fgsea.html) and Gene Set Variation Analysis (https://bioconductor.org/packages/release/bioc/html/GSVA.html)

Graphpad Prism Version 7 was used to perform statistical analysis on kill curves and qPCR.

For manuscripts utilizing custom algorithms or software that are central to the paper but not yet described in the published literature, software must be made available to editors and reviewers upon request. We strongly encourage code deposition in a community repository (e.g. GitHub). *Nature Methods* guidance for providing algorithms and software for publication provides further information on this topic.

Materials and reagents

Policy information about availability of materials

8. Materials availability

Indicate whether there are restrictions on availability of unique materials or if these materials are only available for distribution by a for-profit company.

All analyzed data in this study has been shared in supplementary files. Raw genomics data have been shared with the DBGAP database. All plasmids, cell lines, drugs, chemicals and reagents used in the in vitro studies are common and readily obtainable from commercial sources. In cases where we generated modified plasmids, these will be made available to interested parties.

9. Antibodies

Describe the antibodies used and how they were validated for use in the system under study (i.e. assay and species).

Primary antibodies used: p-HER2 (EMD Millipore – 06-229), HER2 (Cell Signaling Technology – Clone: 44E7 #2248S), ERα (Santa Cruz Biotechnology – Clone: HC-20 #SC-543), p-ERK (1/2) (CST – Clone: E10 #9106S), ERK (1/2) (CST – Clone: 137F5 #4695S), p-AKT (CST – Clone: D9W9U #12694S), AKT (CST #9272S), GAPDH (SCB – Clone: V-18 #SC-20357), β-Actin (Santa Cruz #47778), Goat anti-rabbit (Pierce #32260), Rabbit anti-goat (Invitrogen #81-1620), Goat anti-mouse (Novex #A16090). Primary antibodies were used at a 1:1000 dilution, and secondary antibodies at a 1:2000 dilution. All antibodies used had previously been validated for western blotting in the literature in T47D and MCF7 cell lines.

10. Eukaryotic cell lines

a. State the source of each eukaryotic cell line used.

T47D (American type culture collection #HTB-133), MCF7 cells (ATCC #HTB-22), HEK 293T/17 (American Type Culture Collection #CRL-11268)

b. Describe the method of cell line authentication used.

All cell lines were obtained directly from ATCC as frozen vials. MCF7 and T47D were validated by western blotting for ER and HER2 (based on known genotype).

c. Report whether the cell lines were tested for mycoplasma contamination.

All cell lines tested negative for mycoplasma contamination.

d. If any of the cell lines used are listed in the database of commonly misidentified cell lines maintained by ICLAC, provide a scientific rationale for their use.

No commonly misidentified cell lines were used.

Animals and human research participants

Policy information about studies involving animals; when reporting animal research, follow the ARRIVE guidelines

11. Description of research animals

Provide details on animals and/or animal-derived materials used in the study.

No research animals were used.

Policy information about studies involving human research participants

12. Description of human research participants

Describe the covariate-relevant population characteristics of the human research participants.

This study did not involve a clinical trial and no intervention was performed as part of this research. Tumor and blood samples were obtained from participants with their consent and the approval of the institutional review board, as described in the Methods and Supplementary Methods. All participants were women over the age of 18 who were diagnosed with ER+ breast cancer. Specific patient characteristics including age and details of diagnosis are provided in Figure 1 and in Supplementary Tables 2-4.